Atmosphere–Warm Ocean Interaction and Its Impacts on Asian–Australian Monsoon Variation*

BIN WANG

International Pacific Research Center, and Department of Meteorology, University of Hawaii at Manoa, Honolulu, Hawaii

RENGUANG WU

International Pacific Research Center, University of Hawaii at Manoa, Honolulu, Hawaii

TIM LI

International Pacific Research Center, and Department of Meteorology, University of Hawaii at Manoa, Honolulu, Hawaii

(Manuscript received 5 April 2002, in final form 9 September 2002)

ABSTRACT

Asian–Australian monsoon (A–AM) anomalies depend strongly on phases of El Niño (La Niña). Based on this distinctive feature, a method of extended singular value decomposition analysis was developed to analyze the changing characteristics of A–AM anomalies during El Niño (La Niña) from its development to decay. Two off-equatorial surface anticyclones dominate the A–AM anomalies during an El Niño—one over the south Indian Ocean (SIO) and the other over the western North Pacific (WNP). The SIO anticyclone, which affects climate conditions over the Indian Ocean, eastern Africa, and India, originates during the summer of a growing El Niño, rapidly reaches its peak intensity in fall, and decays when El Nin

cades (Webster et al. 1998; Rao 1999; Kumar et al. 1999). On the other hand, major variations in the east Asian summer monsoon have been found in the year after the El Niño (e.g., Ye and Huang 1996), although there is also a subtle response during the El Niño development (Tanaka 1997). During the year after an El Niño, the summer rainfall over the western North Pacific (WNP) tends to decrease (Wang et al. 2000) while the east Asian subtropical front precipitation tends to enhance (Chen et al. 1992; Chang et al. 2000; Lau and Weng 2001). It was also found that during the mature phase of ENSO (boreal winter), the deficient Australian monsoon rainfall follows a weak Indian summer monsoon (ISM; e.g., Meehl 1987), whereas the rainfall increases over India (Prasad and Singh 1996) and southern China (Zhang et al. 1999).

The monsoon variations in relation to ENSO have been studied largely by linking regional anomalous monsoon rainfall to sea surface temperature (SST) anomalies over the tropical Pacific. Adoption of this popular approach is largely due to the regionality of the monsoon variability and the needs for climate predictions in specific countries. To better understand the linkages of rainfall anomalies in various monsoon subregions and the mechanisms governing year-to-year variations of the A–AM system, it is necessary to examine the season-dependent and ENSO phase-dependent characteristics of the entire A–AM anomalies, including the oceans that are driven by monsoon winds (hereafter monsoon oceans). This is an initial motivation for the present study. In addition, theoretical understanding of the dynamics behind the A–AM variability requires a simple picture that catches the essence of monsoon anomalies. Up till now the existing analyses have not yielded such a picture. This is another incentive of the present study.

A number of mechanisms have been proposed to explain the A–AM variability associated with ENSO. Particular attention has been focused on how the remote El Niño from the eastern equatorial Pacific affects the ISM. By contrasting the monsoon circulation during 1987 and 1988, Nigam (1994) proposed that the oro-

sea interaction in the A–AM variability. Lau et al.'s (2001) numerical experiments demonstrated that the ENSO-induced anomalies in the Bay of Bengal could modulate the latent heat and solar radiation fluxes, leading to SST changes. The atmospheric response to these SST changes opposes the remote response of the south Asian summer monsoon to El Niño warming, thus resulting in a negative feedback in the air–sea coupled loop. Their experiments also imply that the air–sea interaction is not only a cause of local SST variation but also contributes to the Indian monsoon variability.

This paper focuses on discussing the mechanisms whereby the interannual A–AM anomalies associated with ENSO are generated. We start from deriving a simplified picture of the entire anomalous A–AM. For this purpose, a new method, called extended singular value decomposition (ESVD) of covariance is proposed in section 2. We then derive principal modes of the evolving monsoon anomalies associated with the ENSO turnabout in the entire A–AM domain defined as the region from 30°S to 40°N and from 40° to 160°E (section 3). The analysis reveals that the low-level A–AM anomalies are simply characterized by two evolving anticyclones, one located over the south Indian Ocean (SIO) and the other in the WNP. The former dominates during El Niño development while the latter dominates during the mature and decay phases of the El Niño. Rainfall anomalies at various regions of the A–AM are coherent with evolutions of the two anticyclones. In sections 4 and 5, we interpret the results by addressing the following questions: 1) How does the remote El Niño forcing affect the ISM during the initial El Niño development, in particular why is the monsoon anomaly highly asymmetric about the equator? 2) What causes the dramatic amplification of the anomalous SIO anticyclone in the developing phase of El Niño and why can the WNP anticyclone persist during the decay of the El Niño? The last section summarizes major points.

2. Method of extended singular vector decomposition analysis

The singular value decomposition (SVD) analysis is one of the methods that can effectively isolate important coupled modes of variability between two fields (Bretherton et al. 1992). The SVD modes depicts simultaneous coherency between the two fields. Since ENSO has maximum amplitude in northern winter, the signal extracted from SVD analysis of tropical SST and monsoon anomalies is dominated by northern winter pattern (e.g., Lau and Wu 2001). In order to unravel common features of the evolving A–AM anomalies associated with ENSO turnabout, in particular the Asian summer monsoons, we advanced a modified SVD method called extended SVD (ESVD) analysis. The physical basis for such a technique lies in the dependence of A–AM anomalies on the season and the evolution of ENSO.

The idea of ESVD analysis is similar to that of extended EOF analysis (Weare and Nasstrom 1982) except that here we are dealing with covariance analysis of two geophysical fields. Assuming we are interested in the covariability between ENSO turnabout and the associated evolution of the A–AM anomalies, we may make an ESVD analysis with reference to the mature phase of ENSO because the majority of El Niño and La Niña events reach their peaks toward the end of the calendar year (Rasmusson and Carpenter 1982). Based on this strong phase-locking behavior of ENSO turnabout, we used December (0) to February (1) as a reference season for SST anomalies, where 0 and 1 in the bracket denote, respectively, the year during which El Niño develops and the year that follows. We then examine monsoon anomalies in five consecutive seasons from the summer of year 0 [JJA(0)] to the summer of year 1 [JJA(1)]. This evolving scenario takes into account the season-dependent characteristics of the A–AM anomalies and delineates the evolution of the monsoon anomalies with evolving ENSO cycles.

There are a number of parameters in the SVD analysis that deliver important information. The first, which is called the squared covariance fraction, indicates the contribution of each SVD mode to the total covariance between the two analyzed fields (Bretherton et al. 1992). The second important parameter, which is termed as the variance fraction measures the contribution of a derived SVD mode to the total variance of each individual field. For each field, the ratio of the variance associated with an SVD mode to the corresponding total variance defines the variance fraction. In general, the variance fractions computed for the two fields are different.

In the ESVD analysis, because the element of the second field contains a suite of consecutive steps {in our interest, seasonal mean A–AM anomalies in June–July–August [JJA(0)], September–October–November [SON(0)], December–January–February [D(0)/JF(1)], March–April–May [MAM(1)], and June–July–August [JJA(1)]}, it is necessary to compute variance fractions for each time step (season), which provides additional information indicating the relative amplitudes of the A–AM anomalies accounted for by the ESVD mode at differing phases associated with the ENSO turnabout. Likewise, the squared covariance fractions for each step compare the relative amplitudes of the covariance between the mature phase SST and A–AM anomalies accounted for by the ESVD mode at differing phases of ENSO.

We analyzed winds at 850 hPa, sea level pressure, and vertical *p*-velocity at 500 hPa derived from the National Centers for Environmental Prediction–National Center for Atmospheric Research (NCEP–NCAR) reanalysis (Kalnay et al. 1996) for the period of 1958–99. These data are on regular grids with a horizontal resolution of 2.5° × 2.5°. The skin temperature and precipitation are derived from the NCEP–NCAR reanalysis on Gaussian grids of T62 with a horizontal resolution of about 1.9° × 1.9°. Over the open ocean, the skin temperature is fixed at the Reynolds SST (Reyn-

olds and Smith 1994). To focus on the interannual variation, we removed decadal–interdecadal variations (periods exceeding 8 yr) from the raw data.

3. Evolution of A–AM anomalies associated with the ENSO turnabout

Figure 1 shows the evolution of A–AM anomalies in five consecutive seasons associated with ENSO peak SST anomalies by the principal ESVD mode. This mode describes 91% of the total covariance between the mature phase SST anomalies in the tropical Pacific and Indian Oceans (20°S–20°N, 40°E–90°W) and the total five seasonal mean 850-hPa wind anomalies in the A–AM domain (30°S–40°N, 40°–160°E). The correlation coefficient between the temporal coefficients of the two fields is 0.94. The SST anomalies associated with the dominant ESVD mode accounts for 68% of the total interannual variances of the D(0)/JF(1) SST anomalies, while the variance fraction of the A–AM anomalies for the five seasons and over the entire A–AM domain (30°S–40°N, 40°–160°E) accounts for 18% for 850-hPa winds. Similar ESVD analyses of the SST–500-hPa vertical velocity and SST–sea level pressure were carried out. The derived dominant mode of SST anomalies is extremely similar with that shown in Fig. 1f. To save space, we plot the corresponding 500-hPa vertical *p*-velocity anomaly fields together with the 850-hPa wind anomaly fields and present the sea level pressure anomalies in Fig. 2.

Note that the variance fractions of the A–AM anomalies averaged for the entire domain vary with seasons. For the 850-hPa winds and 500-hPa vertical motion, the largest fraction variances are found in the fall of the El Niño (or La Niña) developing year, which is 30% for the 850-hPa zonal wind and 18% for the 500-hPa vertical velocity. The fraction variances for the sea level pressure anomalies accounts for 33% and 39% of the total variances in the SON(0) and D(0)/JF(1), respectively.

Note also that the fractional variances of the A–AM anomalies accounted for by this ESVD mode vary remarkably with locations. Figure 3 presents geographic distributions of the variance fraction computed based on the first ESVD mode for the 850-hPa zonal wind (Fig. 3a) and 500-hPa vertical velocity (Fig. 3b). The regions of high variance fraction denote the locations where the most robust influence of ENSO occurs. For the 850-hPa zonal wind, a high variance fraction region of an anomalous westerly over the western Pacific moves eastward from JJA(0) to SON(0); meanwhile, a high variance fraction region of easterly anomalies occurs over the eastern equatorial Indian Ocean in SON(0), intensifies, and moves eastward in D(0)/JF(1), and then weakens and moves northward in MAM(1) and JJA(1) (Fig. 3a). Another high variance fraction region is located over the southeast China coast in D(0)/JF(1) and MAM(1), indicating enhanced westerly anomalies south of the east Asian polar front. As far as the 500-hPa vertical motion is concerned, a high variance fraction region (suppressed convection) initially establishes over the Maritime Continent in JJA(0), rapidly intensifies, and expands in SON(0), and then moves northeastward to the Philippine Sea from D(0)/JF(1) to JJA(1), indicating that the subsidence in the mature and decay phases of El Niño over the Philippine Sea is a robust signal (Fig. 3b).

During the summer when El Niño develops, an elongated anticyclonic ridge extending from the Maritime Continent to the southern tip of India dominates the low-level circulation anomaly (Fig. 1a). Associated with this ridge are pronounced westerly anomalies expanding from the Bay of Bengal to WNP and a region of enhanced convection over the Philippine Sea as well as a region of suppressed convection over the Maritime Continent. There is a sign of the weakening of the local meridional circulation between the Maritime Continent and the Philippine Sea. The eastward extension of the WNP monsoon trough increases the number of tropical storm formations in the southeast quadrant of the tropical WNP (5°–17°N, 140°–170°E; Wang and Chan 2002; Chen et al. 1998). On the other hand, the weak anticyclonic anomalies found over peninsular India imply a deficient ISM. Note that to the southwest of Sumatra convection is severely suppressed and the surface pressure rises (Figs. 1a and 2a), which induces a notable cross-equatorial flow west of Sumatra and a weak anticyclonic cell over the SIO.

During the fall of the El Niño developing year (Figs. 1b and 2b), the SIO anticyclone has grown explosively, resulting in a massive anticyclonic ridge dominating the entire Indian Ocean with a titled ridge extending from western Australia all the way to the Somalia coast; westward surface pressure gradient and intense easterly anomalies build up along the equatorial Indian Ocean; and descent (ascent) enhances over the eastern (western) Indian Ocean. The most suppressed convection is located slightly to the eastward and equatorward of the anticyclone center, suggesting the anticyclone is a Rossby wave response to the suppressed heating (descent). Over the western Maritime Continent, easterly anomalies and drought conditions further grow, while over the western Pacific westerly anomalies progress eastward toward the central Pacific. A notable new anomalous anticyclone starts to form in the vicinity of the northern Philippines (Fig. 2b).

In the mature phase of El Niño, D(0)/JF(1), the monsoon anomalies are dominated by two subtropical anticyclonic systems, one is located over the SIO and the other over the WNP (Fig. 1c), which correspond to the high pressure anomalies over the southeast Indian Ocean and the Philippine Sea (Fig. 2c). The former results from the weakening and southeastward retreat of the SIO anticyclone, while the latter is a result of the rapid amplification and eastward migration of the Philippine an-

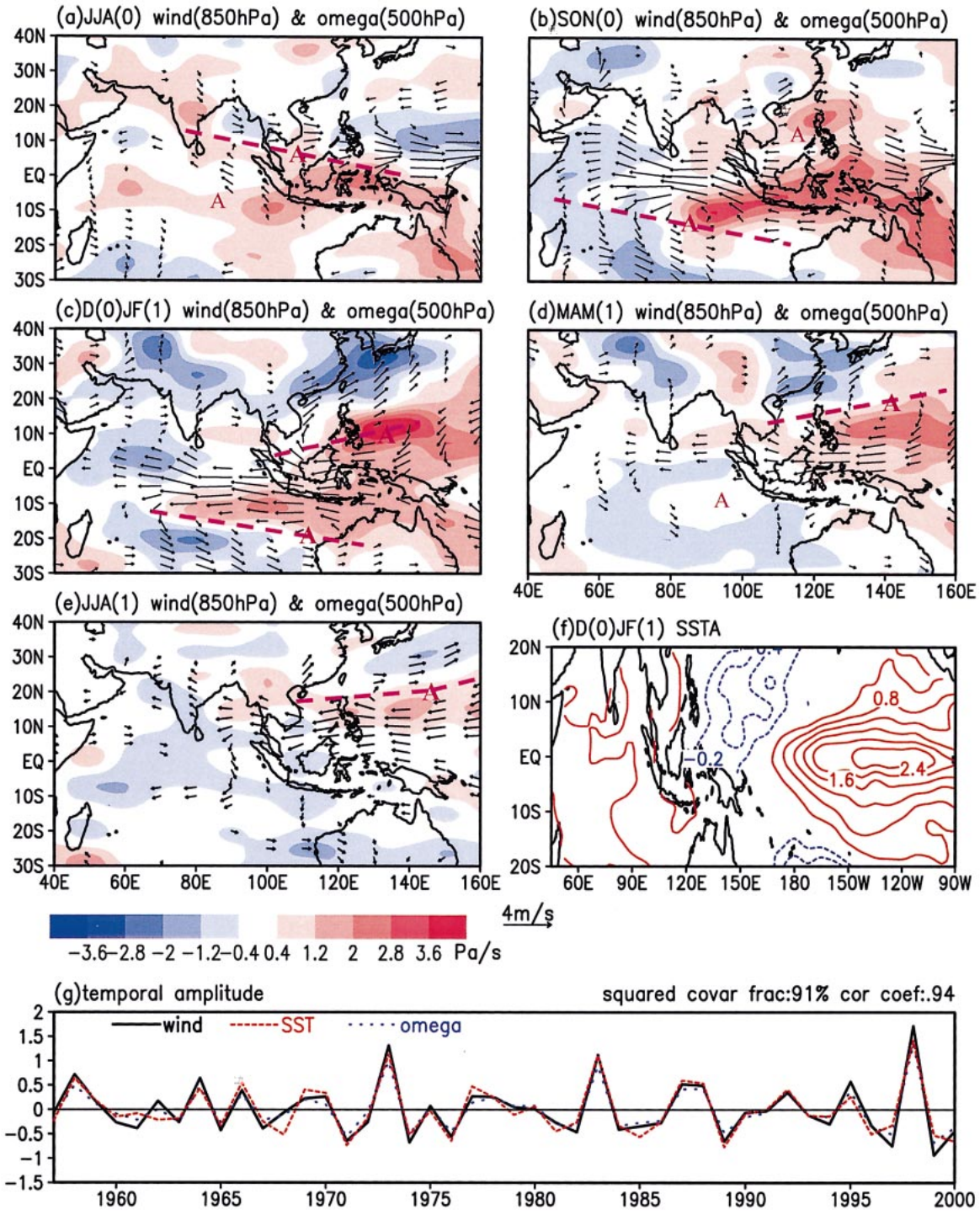

FIG. 1. (a)–(f) The spatial patterns of the dominant ESVD mode and (g) the corresponding time coefficients of the wind and SST anomalies. (a)–(e) The seasonal mean 850-hPa winds (vectors) and 500-hPa vertical *p*-velocity (color shading) from JJA(0) to JJA(1), where year 0 and year 1 denote the year during which an El Niño develops and the following year, respectively. Only wind anomalies significant at the 95% confidence level are shown. (f) Seasonal mean SST anomalies in D(0)/JF(1). The numbers on the top-right of (g) are the squared covariance fraction between wind and SST anomalies (0.91) and the correlation coefficient between the two time series (0.94).

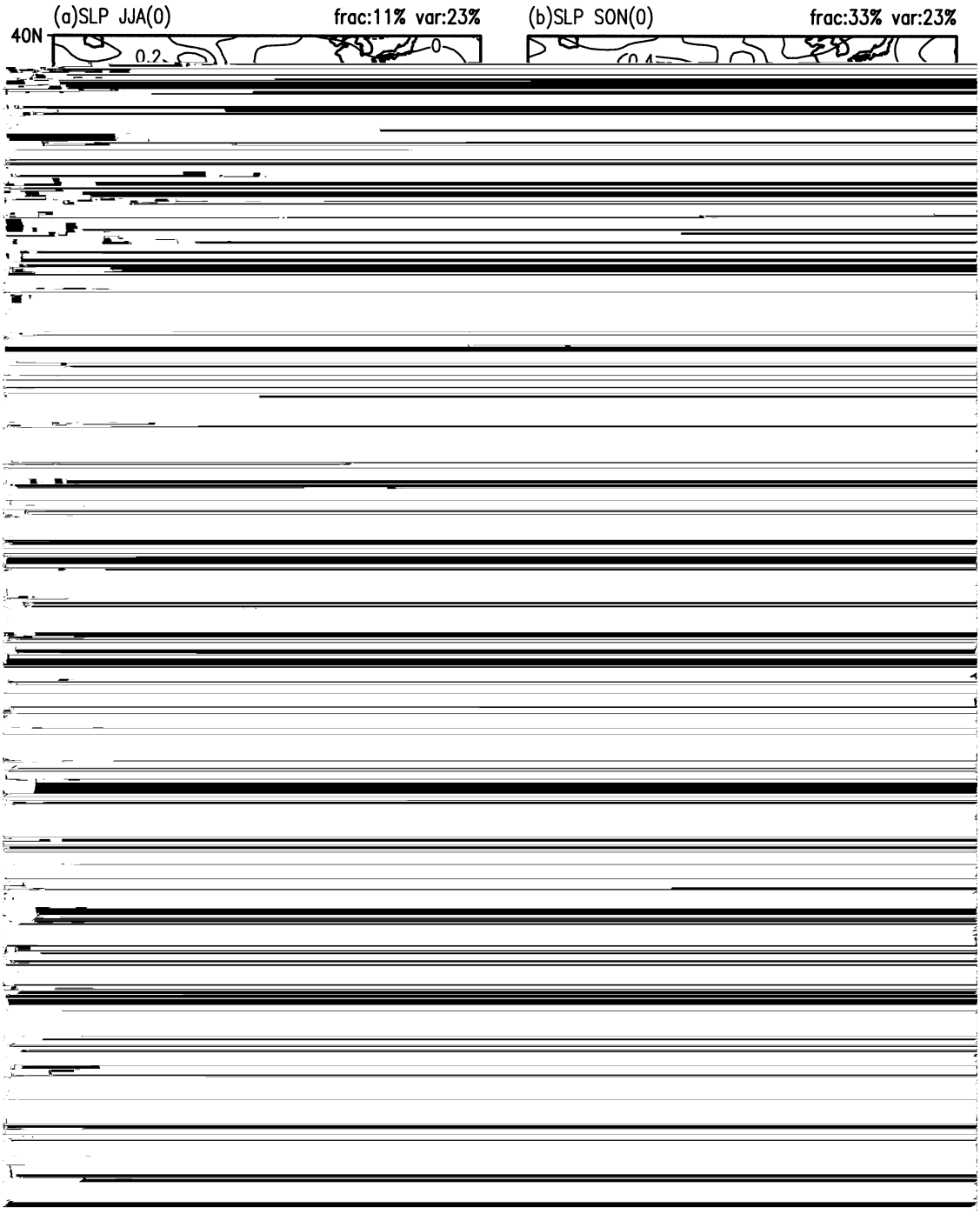

FIG. 2. The same as in Fig. 1 except for the sea level pressure anomalies rather than the wind and vertical motion anomalies. Shading indicates areas where the sea level pressure anomalies are significant at the 95% confidence level. The numbers on the top-right of (g) are the squared covariance fraction between sea level pressure and SST anomalies (0.93) and the correlation coefficient between the two time series (0.95).

ticyclone. The driest area shifts from the Maritime Continent to the Philippine Sea, although the Indonesian–Australian summer monsoon region remains to be controlled by subsidence. The two massive anomalous anticyclones imply a weakened A–AM system, especially the weakening of the east Asian winter monsoon and the Australian summer monsoon. Enhanced precipitation is found over the western equatorial Indian Ocean and the east Asian polar frontal zone (southern China–Kyushu Island of Japan). Along the equator, both the

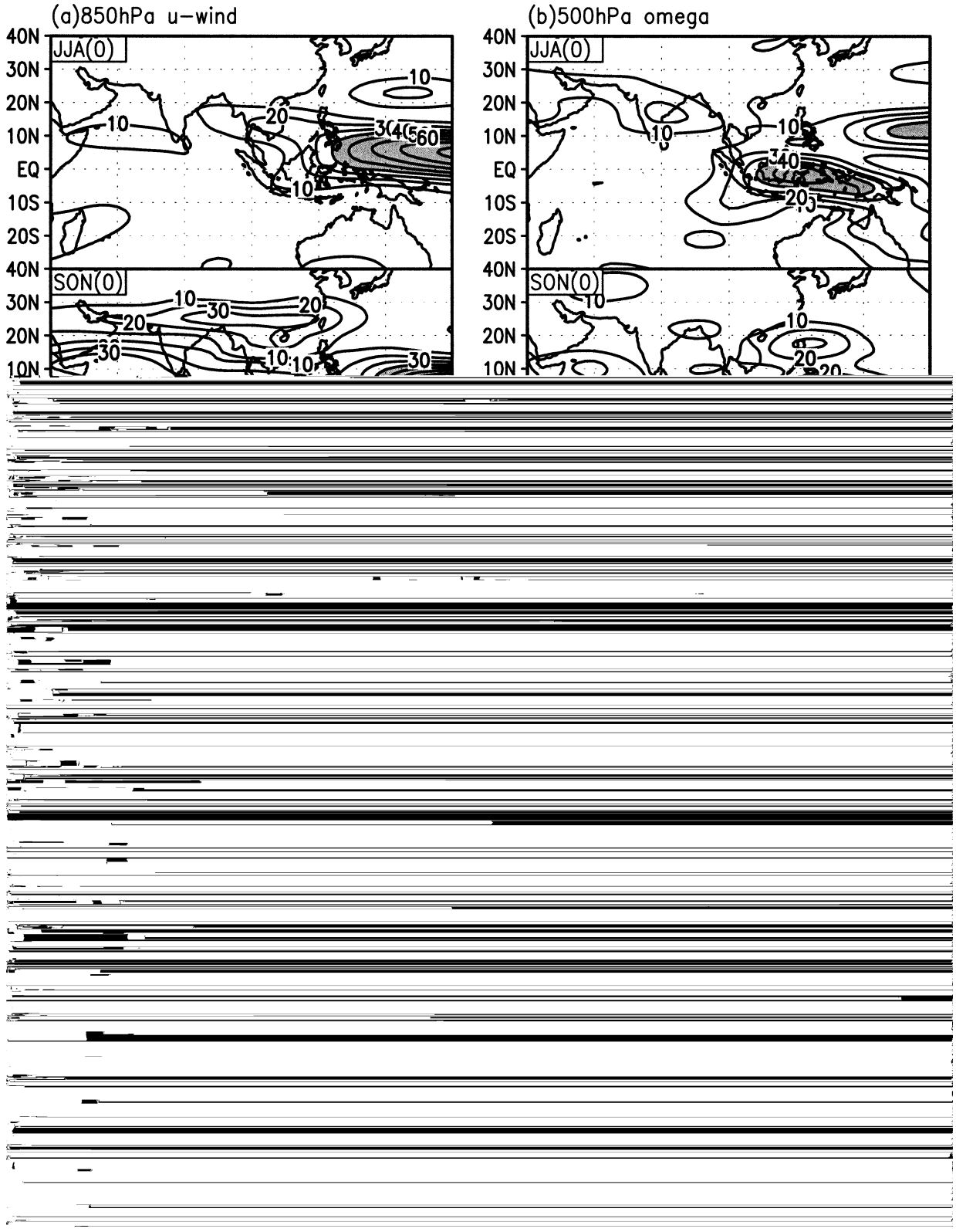

FIG. 3. Distribution of the variance fraction accounted for by the dominant ESVD modes for the (a) 850-hPa zonal wind and (b) 500-hPa vertical *p*-velocity anomalies. The contour interval is 10%. Shading indicates a variance fraction over 40%.

Indian Ocean easterly anomalies and the western Pacific westerly anomalies move farther eastward.

The anomalies in MAM(1) and JJA(1) exhibit similar patterns, which are characterized by the pronounced WNP anticyclone (Figs. 1d and 1e) and enhanced surface pressure (Figs. 2d and 2e). The intensity of the WNP anticyclone, however, decreases toward JJA(1). During JJA(1), anomalous subsidence controls the Philippine Sea and Southeast Asia, signifying a weakening of the summer monsoon over the WNP and Southeast Asia.

Comparison of Figs. 1a (2a) and 1e (2e) reveals that from JJA(0) to JJA(1), all the anomaly patterns in the 850-hPa winds, 500-hPa vertical motion, and sea level pressure nearly reverse their corresponding polarities in the tropical Indian and western Pacific Oceans between 10°S and 20°N. This indicates a strong biennial tendency of the A–AM variability associated with the El Niño turnabout.

The most important feature of the A–AM anomalies is the evolution of the two anomalous anticyclones that are located, respectively, over the SIO from the developing to mature phase and over the subtropical WNP from the mature to decay phase of El Niño. To understand the A–AM anomalies, one must address the questions concerning the origin, development, and maintenance of the SIO and WNP anomalous anticyclones. We suggest that the observed A–AM anomalies are attributed to two factors, the direct remote El Niño forcing and the local monsoon–ocean interaction.

4. Remote ENSO forcing and effects of the monsoon mean circulation

The impacts of the remote El Niño forcing may be best exemplified by the anomalous monsoon observed in JJA(0) (Fig. 1a), because the warming in the eastern Pacific is in an early developing stage (Fig. 4a). Consistent with the previous studies, the remote forcing from the eastern Pacific warming shifts the Walker circulation eastward and suppresses convection over the Maritime Continent. According to the Matsuno (1966)–Gill (1980) theory, the suppressed convection over the Maritime Continent would excite an equatorial symmetric Rossby wave response and form twin low-level anticyclones residing on each side of the equator and to the west of the heat sink. The observed pattern in Fig. 1a, however, shows a remarkable asymmetry of the low-level anticyclonic anomalies with respect to the equator. How can this equatorial asymmetry be explained?

We propose that the equatorial asymmetric response results from the effects of monsoon mean flows on the equatorial Rossby wave response. Wang and Xie (1996) and Xie and Wang (1996) extended Matsuno's equatorial wave theory and investigated the effects of three-dimensional background circulations on equatorial waves. Their normal mode analyses demonstrate that easterly vertical shears can drastically amplify moist Rossby waves while westerly shears tend to reduce them. The reasons follow. In the presence of a vertical shear, the convective heating directly stimulates the baroclinic Rossby mode, and then generates the barotropic Rossby mode through vertical shear-induced coupling between the two vertical modes. Under easterly (westerly) shears, the sum of the two modes results in an enhanced (reduced) circulation in the low level. Thus, the Rossby waves in the easterly shear interact with convective heating more vigorously through boundary layer Ekman flow-induced moisture convergence or divergence. As such, the moist equatorial Rossby wave response in the presence of easterly vertical shear is substantially stronger than that under westerly shears. Using an intermediate tropical atmospheric model, Wang and Xie (1997) confirmed the crucial roles of the 3D background flows in regulating the equatorial wave behavior. The 3D monsoon flows include not only vertical shears but also horizontal shear and vertical motion. They examined contributions from each of these factors by sensitivity experiments and found the vertical shear to be the most effective factor in determining the outcome of the wave response.

Figure 5 shows the distribution of the vertical shear (200 − 850 hPa) of the zonal winds in boreal summer and winter. In boreal summer, the monsoon easterly vertical shear favors the suppressed Maritime Continent convection that generates moist descending Rossby waves with large amplitude in the low level. This explains why the JJA(0) monsoon anomalies are dominated by an anticyclonic ridge located north of the equator, while the response in the Southern Hemisphere is weak (Fig. 1a). On the other hand, during the mature phase of El Niño, the suppressed convection over the Maritime Continent and Australian monsoon region would favor anomalous anticyclones forming over the tropical SIO. We note that, over the WNP, the low-level anticyclone is located in an unfavorable environment of weak westerly shear, thus other factors must come into play in order to account for the rapid intensification. This point will be further elaborated in section 5.

To validate the effects of the mean flow, we conducted a numerical experiment with an anomaly AGCM. Choice of a multilevel linearized AGCM is more realistic because three-dimensional basic states can be specified. Our anomaly model was constructed based on the dynamic core of the Geophysical Fluid Dynamics Laboratory AGCM, which is similar to the one used by Ting and Yu (1998). A 3D summer mean (JJA) basic state is prescribed in an equally distributed five-level sigma coordinate. A strong momentum damping with a decaying timescale of 1 day is applied in the lowest model level to mimic the planetary boundary layer dissipation, while a Newtonian damping of an *e*-folding timescale of 10 days is applied to all levels in both momentum and heat equations.

Figure 6 illustrates the response of the lowest-level

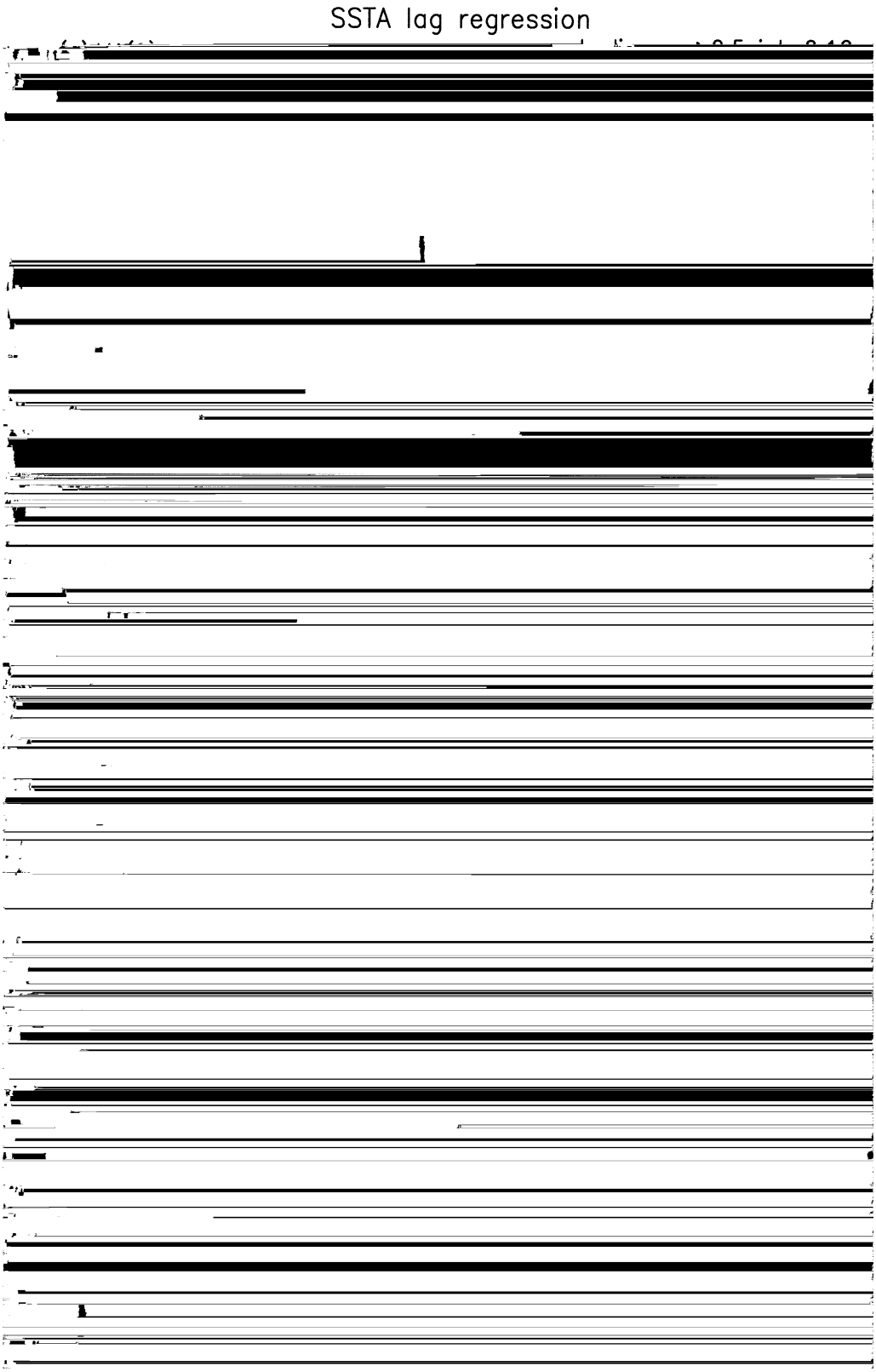

FIG. 4. Five consecutive seasonal mean SST anomalies derived using lag regression with reference to the time coefficient of the SST anomalies in the dominant ESVD mode. Shading indicates regions where the correlation coefficient exceeds 0.5.

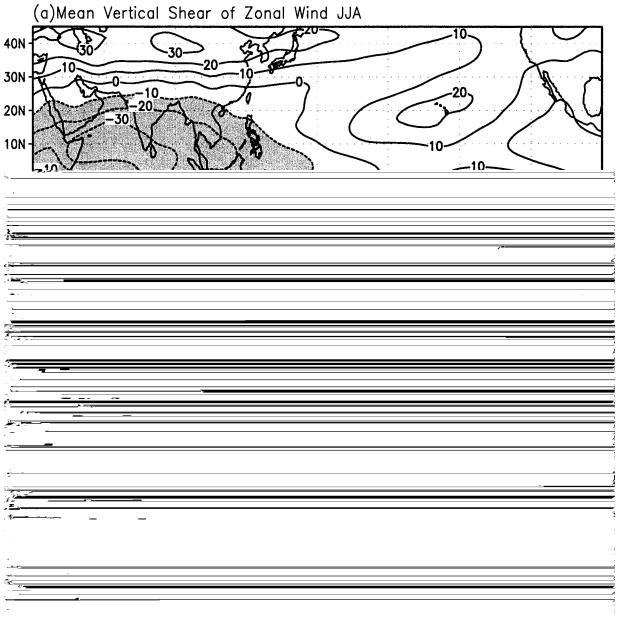

FIG. 5. Distribution of mean vertical shear (200 − 850 hPa) of zonal winds derived for the period 1957–2000 in (a) boreal summer and (b) winter. Shading denotes easterly shear exceeding 10 m s^{-1}.

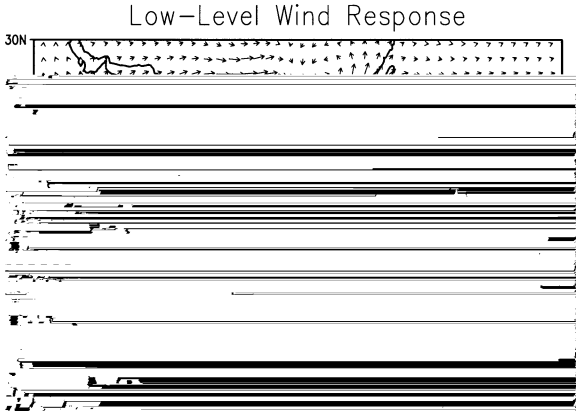

FIG. 6. The low-level wind response to an equatorial symmetric heat sink simulated by using a linearized AGCM with specified realistic 3D mean summer (JJA) basic state. The contours represent horizontal distribution of the heat sink strength at an interval of 0.4°C day^{-1} with maximum amplitude of the heating rate of -2°C day^{-1}, which is located in the midtroposphere.

winds to a prescribed ideal equatorial symmetric heat sink. In the presence of the realistic 3D summer mean flow, the atmospheric response is obviously asymmetric to the equator—a strong low-level anticyclone anomaly appears to the north of the equator. The anomalous anticyclone extends to the west of the heat sink, covering the entire south Asian monsoon region. On the other hand, with specification of a rest background flow, the model produces a symmetric response with twin anticyclones residing on each side of the equator (figure omitted). When the mean winter (DJF) basic flow is specified, the model simulates a stronger anticyclonic response in the Southern Hemisphere, consistent with the distribution of the easterly vertical shear. The numerical results support the theory that the monsoon background flows play a critical role in modifying the A–AM response to anomalous El Niño forcing.

Figure 1a shows a more complicated 500-hPa sinking motion pattern over the Maritime Continent than that used in numerical experiments with an AGCM (Fig. 6). However, our ideal numerical experiment is based on the following assumption: The Pacific warming is an equatorial phenomenon and the induced sinking branch of the anomalous Walker circulation is primarily symmetric about the equator centered on the equatorial Maritime Continent. The experiment demonstrates that even though the remote El Niño impact is equatorial symmetric, the response of the atmosphere in the presence of the monsoon basic flows is highly biased to the Northern Hemisphere due to asymmetric Rossby wave response to the monsoon mean flows. We argue that once the descending Rossby waves are generated by the heat sink, they will affect adjacent atmospheric convection and vertical motion. Thus, the observed 500-hPa vertical *p*-velocity anomalies (Fig. 1a) may extend westward (from the suppressed Maritime Continent convection) into the Bay of Bengal and India and into the south Indian Ocean. Arguably, the suppressed convection formed in the off-equatorial regions would further feed back to the local circulation anomalies and induce a more complicated sinking motion pattern. This implies that the observed complex pattern of descending motion (Fig. 1a) may in part be due to the asymmetric response in the presence of the monsoon mean flows.

5. Roles of atmosphere–ocean interaction

Figure 4 indicates that the warming in the eastern Pacific develops in the boreal summer of year (0), reaches its height in the following winter, and disappears in the ensuing summer. The strength of the remote El Niño forcing from the eastern Pacific is assumed to be proportional to the intensity of the warm SST anomalies. This assumption is consistent with the sea level pressure anomalies around the Maritime Continent (Fig. 2).

In the Indian sector (40°–105°E), the monsoon anomalies are stronger in SON(0) than in the mature phase of ENSO when the remote El Niño forcing is the strongest (Figs. 1b and 1c). The mismatch between the strengths of the Indian monsoon anomalies and the remote El Niño forcing suggests that the remote forcing alone is unable to explain the evolution of the Indian monsoon anomalies. In the east Asian sector (105°–160°E), pronounced anticyclonic anomalies occur over the Philippine Sea in MAM(1) and JJA(1) after the mature phase of ENSO (Figs. 1d and 1e). Because the remote forcing in the eastern Pacific decays rapidly in MAM(1) and even reverses its sign in JJA(1) (Figs.

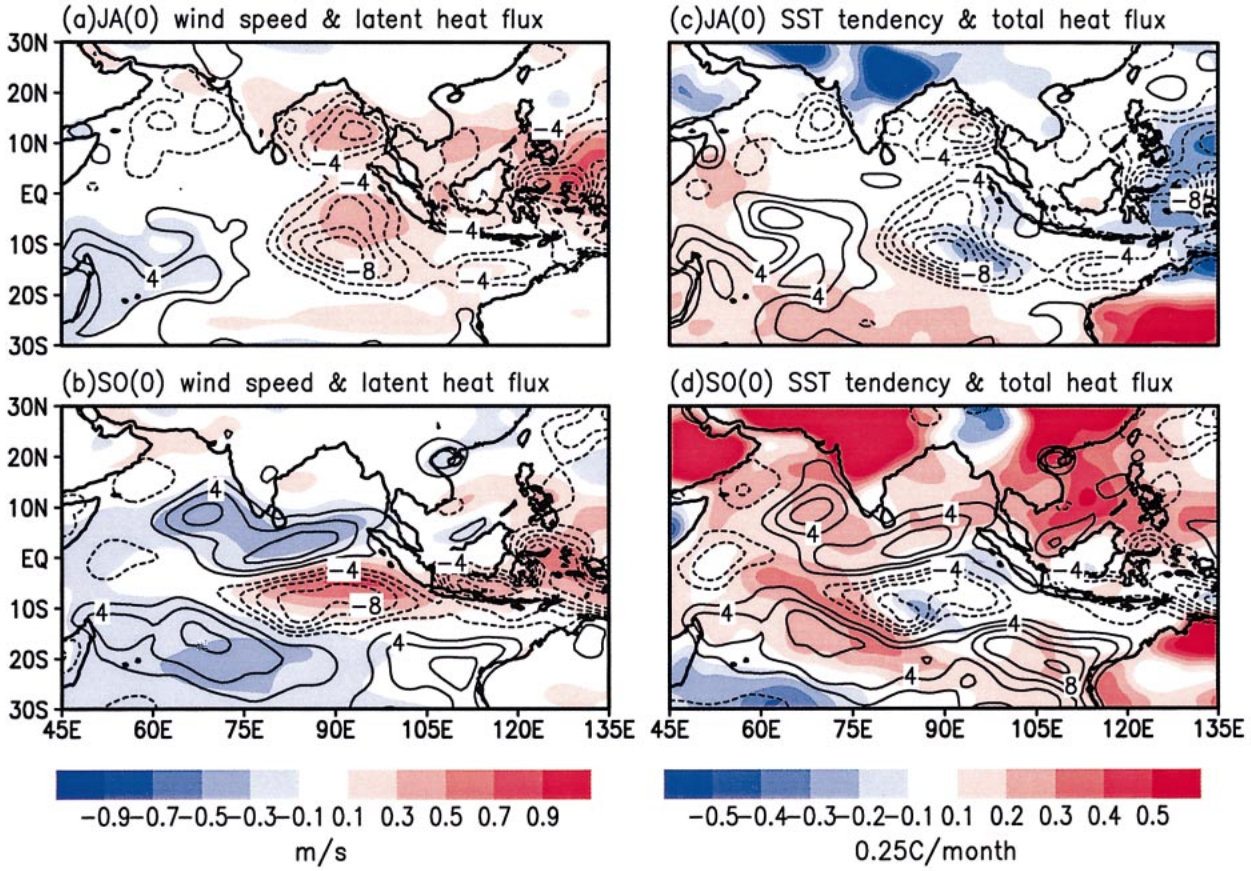

FIG. 7. (a), (b) The anomalous surface wind speed (m s^{-1}, color shading) and downward latent heat flux (contour) in JA(0) and SO(0), respectively. (c), (d) The SST tendency (color shading) and total downward surface heat flux (contour) anomalies in JA(0) and SO(0), respectively. The heat flux contour interval is 2 W m^{-2}.

4d,e), the maintenance of the WNP anticyclone cannot also be elucidated by the remote El Niño forcing.

We suggest that the atmosphere–ocean interaction plays a crucial role in the drastic amplification of the SIO anticyclone while El Niño develops and in the long-lasting persistence of the WNP anticyclone while El Niño decays.

a. Atmosphere–ocean interaction over the Indian Ocean

From the oceanographic point of view, under summer monsoon background flows, the anomalous SIO anticyclone causes cooling in the eastern Indian Ocean and warming in the western basin. The SIO anticyclone enhances southeasterly winds off the coast of Sumatra that increase the coastal and equatorial upwelling (Saji et al. 1999; Murtugudde et al. 2000). Away from the coast, the anomalous SIO anticyclone increases (decreases) wind speed to the east and west of the anticyclone (shadings in Figs. 7a,b), which results in enhanced (reduced) evaporation and entrainment cooling in the tropical southeastern (southwestern) Indian Ocean (contours in Figs. 7a,b). Figures 7c and 7d indicate that the evaporation flux has a prevailing contribution to the total downward surface heat flux, because they have similar patterns. Figures 7c and 7d also show that the Indian Ocean SST tendency has an overall pattern similar to that of the total downward surface heat flux, suggesting the importance of the anomalous SIO anticyclone-induced heat flux in generating large-scale SST anomalies. This assertion, based on observational evidence, is in good agreement with results obtained in some numerical model experiments (e.g., Behera et al. 2000; Murtugudde et al. 2000). Thus, the SIO anticyclone is responsible for the SST dipole pattern with cold water to the east and warm water to the west of the SIO center. Note, however, in some regions the total downward heat flux does not correspond to the SST tendency. This may be due to inaccuracy in the reanalysis data and use of monthly SST values, but more likely it suggests that ocean dynamic processes play decisive roles. For instance, near 10°S and 70°W in JA(0), the positive heat flux does not correspond to a warming trend. Xie et al. (2002) showed that the downwelling oceanic Rossby waves generated by equatorial easterly anomalies deep-

en the thermocline; meanwhile the local wind stress curl induces downwelling, both causing warm SST anomalies in that region. The suppression of coastal and equatorial upwelling may significantly contribute to the warming over the Arabian Sea and the west equatorial Indian Ocean. The Indonesian throughflow, which carries colder water, could raise the thermocline and increases the Java–Sumatra upwelling-induced cooling (Susanto et al. 2001). The effects of the freshwater flux on creating a barrier layer may play a role in maintaining the western basin warming (Saji et al. 1999; Murtugudde et al. 2000; Annamalai et al. 2002, hereafter AMPXW).

From a meteorological point of view, the SST dipole anomaly can enhance the SIO anticyclone. The enhanced ocean surface cooling off the coast of Sumatra may reduce convective instability and increase the sea level pressure (Zebiak 1986; Lindzen and Nigam 1987; Wang and Li 1993), favoring suppressed convection. This local ocean feedback process has been confirmed by numerical experiments with the Center for Ocean–Atmosphere–Land Studies (COLA) AGCM, which demonstrate that a local negative SST anomaly in the warm pool ocean reduces local rainfall (Wang et al. 2000). The suppressed convection, which is situated southwest of Sumatra, can stimulate descending Rossby waves, which would enhance the low-level anomalous anticyclone in their decaying journey to the west (Gill 1980). Likewise, in the western Indian Ocean the sea surface warming can strengthen convection, so that a convection dipole forms with dry conditions to the east and wet conditions to the west of the SIO anticyclone.

The aforementioned observation and model results suggest a positive feedback between the SIO anticyclone and SST dipole in the presence of the boreal summer monsoon flows, which provides a growing mechanism for the SIO anticyclone from boreal summer to fall while El Niño develops (Fig. 1b).

Note that the above-described positive feedback depends critically on boreal summer monsoon background flows. Once the summer monsoon changes to the winter monsoon after November, the background flows reverse direction north of the SIO convergence zone (along 10°–15°S), which would switch the positive feedback to a negative one. Therefore, the cold pool off the coast of Sumatra decays rapidly and sometimes transforms to a weak warming. This explains why the southeast Indian Ocean cooling reaches a maximum intensity in boreal fall (Fig. 4b; Saji et al. 1999).

b. The atmosphere–ocean interaction over the western North Pacific

In the east Asian sector, the WNP anticyclone was initiated in SON(0) (Fig. 1b). Wang and Zhang (2002) have attributed the establishment of the anomalous anticyclone to a number of factors: remote El Niño forcing, extratropical–tropical interaction, and local air–sea interaction associated with the intraseasonal oscillation. For details the readers are referred to that paper. The WNP anticyclone rapidly amplifies from fall to winter (Fig. 1c). Given the fact that the northern winter westerly shears prevailing over the WNP (Fig. 5b) are not favorable for the development of the anticyclonic anomalies, how could the WNP anticyclone amplify rapidly? More importantly, in the ensuing spring and summer when the remote El Niño forcing continues to decay, what mechanisms can maintain the WNP anticyclone through the next spring and summer? Wang et al. (2000) have attributed the development and persistence of the WNP anticyclonic anomaly to a positive thermodynamic feedback between the anomalous WNP anticyclone and the underlying warm pool ocean. Figures 8a and 8b show that in the presence of northeasterly trade winds and the Asian winter monsoon, the increased (decreased) total wind speed to the southeast (northwest) of the anomalous anticyclone center induces excessive (moderate) evaporation and entrainment cooling. Figures 8c and 8d further show that the total downward surface heat flux has a similar pattern as that of the latent heat flux with some modification due mainly to the anomalous solar radiation flux (for brevity the solar flux is not shown). Thus the WNP anticyclone anomalies generate the SST dipole with cold water to the east and warm water to the west of the anticyclone (Figs. 1c,d and 4c,d). The cooling to the east of the WNP anticyclone, in turn, suppresses convection and reduces latent heat release, which excites descending atmospheric Rossby waves that propagate westward and reinforce the WNP anomalous anticyclone. This hypothesis has been verified by numerical experiments of Lau et al. (2001). They employed a coupled Geophysical Fluid Dynamics Laboratory AGCM–mixed layer ocean model and demonstrated that the interaction of the atmosphere and mixed layer ocean can indeed amplify and sustain the anomalous anticyclone over the subtropical WNP.

6. Summary

a. Observational findings

The Asian–Australian monsoon (A–AM) anomalies depend on the seasonal march and the phases of the ENSO cycle. We therefore proposed a new technique, the extended singular value decomposition (ESVD) analysis, to depict the A–AM anomalies associated with the ENSO changeover from development to decay years.

Our analysis yields a simple picture about the evolution of the A–AM anomalies associated with an El Niño event, namely, the low-level monsoon anomalies are characterized by two off-equatorial anomalous anticyclones: one located over the south Indian Ocean (SIO) and the other over the western North Pacific (WNP; Fig. 1). Significant vertical motion and equatorial wind anomalies are intimately associated with the evolution of the two anticyclones (Fig. 3). This simplified picture is believed to be useful for theoretical

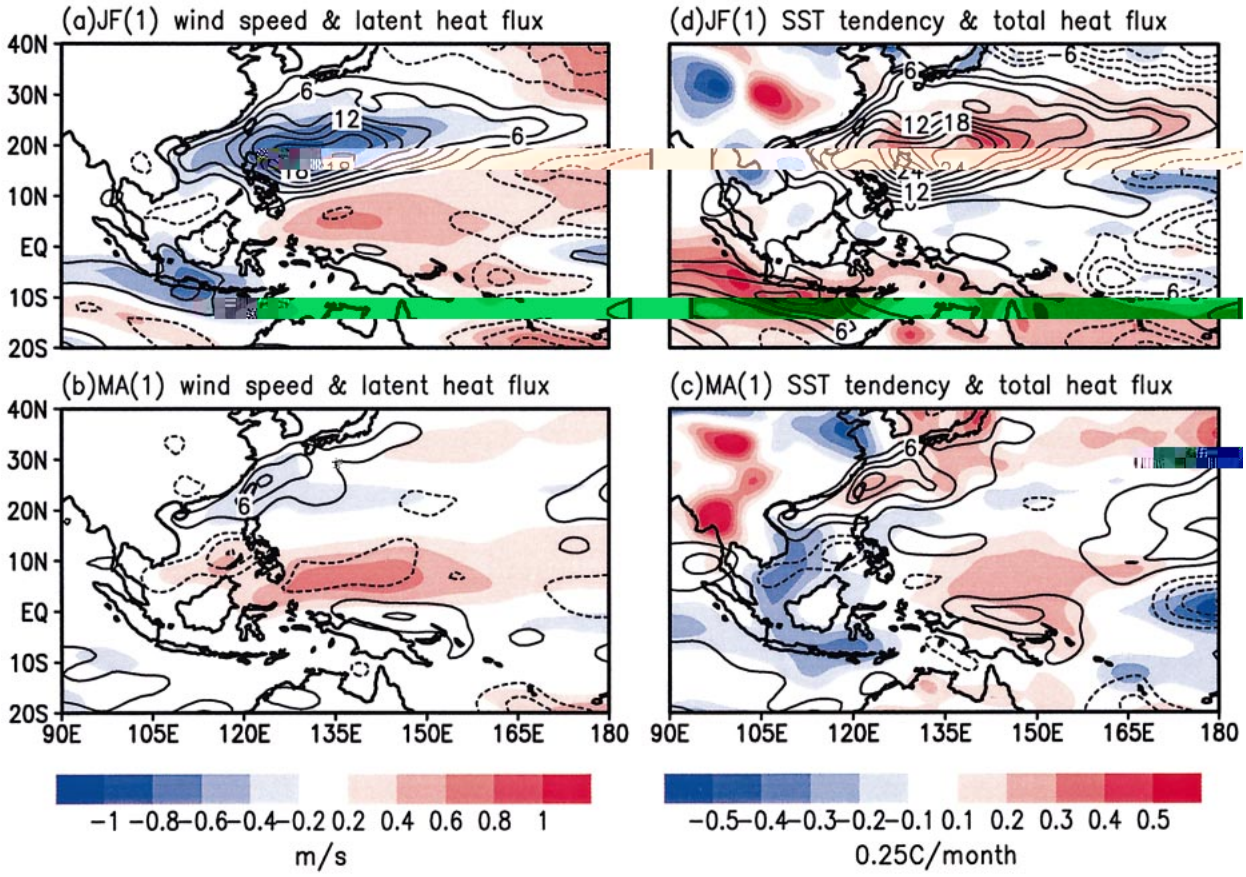

FIG. 8. Same as Fig. 7 except for JF(1) and MA(1) and the heat flux interval is 3 W m^{-2}.

understanding of the fundamental physics whereby El Niño impacts the A–AM system.

The SIO anticyclone, which causes rainfall anomalies over the Indian Ocean, East Africa, and India, is initiated southwest of Sumatra in the boreal summer while an El Niño develops, rapidly reaches its height in the fall, and persists into the mature phase of El Niño with a decreased intensity (Figs. 1a–c). On the other hand, the WNP anomalous anticyclone, which is responsible for precipitation anomalies over east Asia, Southeast Asia, and the WNP, forms near the northern Philippines in the fall of the El Niño developing year, attains its peak in the mature phase of El Niño, and persists through the next spring and summer notwithstanding the decay of El Niño (Figs. 1b–e).

Figures 1 and 2 also reveal that from the development to the decay phase of El Niño, the largest variability of the A–AM system shifts from the tropical southern Indian Ocean to the western North Pacific. This confirms the results of an earlier analysis of the sea level pressure evolution during composite El Niño (Wang 1995). Overall, El Niño (La Niña) tends to weaken (enhance) the entire A–AM system defined over the domain (30°S–40°N, 40°–160°E) with the strongest weakening of the low-level winds and vertical motion being found during the fall of El Niño development.

A strong biennial tendency is found to be associated with the turnabout of El Niño and La Niña events. The anomalous sea level pressure, 850-hPa winds, and 500-hPa vertical motion in the region (10°S–20°N, 40°–160°E) during the summer of El Niño development are nearly reversed compared to their counterparts during the summer of El Niño decay. This result reveals the action centers of the tropospheric biennial oscillation (TBO) of the A–AM system and suggests its close linkage with the ENSO turnabout. It is instrumental for us to further understand the nature of the TBO of the ENSO–A–AM system.

The ESVD analysis contains both El Niño and La Niña phases. It reflects the mean differences of monsoon anomalies associated with the El Niño and La Niña events. The underlying presumption is that the monsoon anomalies associated with a La Niña resemble those of an El Niño but with opposite polarities. This has been confirmed by composite analyses of the A–AM anomalies for 11 El Niño events and 9 La Niña events in the last 50 yr (figure not shown).

We have shown observed evidence that the SIO and

WNP anticyclones, being superposed upon their respective winter background flows, increase (decrease) wind speed thus evaporation/entrainment cooling in the east (west) of the anticyclone center (Figs. 7a,b and 8a,b). In the two anticyclone regions, the anomalous surface latent heat fluxes have a leading contribution to corresponding total downward surface heat flux anomalies and play a fundamental role in generating the large-scale dipole SST anomaly patterns (Figs. 7 and 8). Therefore, the anomalous atmosphere–ocean conditions over the two anticyclone regions are similar: warm water to the west and cold water to the east of the anticyclone center (Fig. 9).

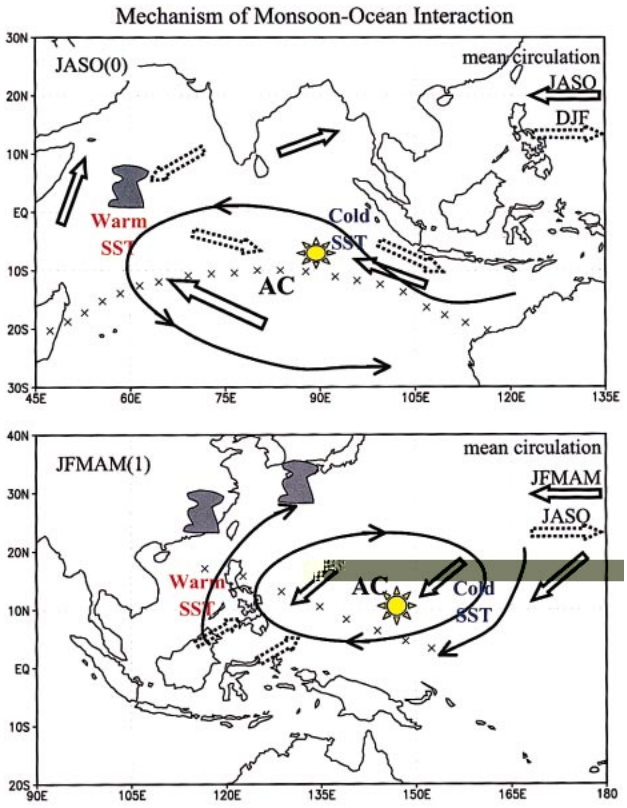

FIG. 9. Schematic diagrams showing the essential dynamics of the coupled monsoon–ocean modes over (a) the SIO and (b) the WNP. A positive feedback exists between the anomalous atmospheric anticyclone and SST dipole [warm (cold) to the east (west) of the anticyclone center] in the presence of the mean circulation during local winter and spring (solid double arrows). See text for the discussion of the positive feedback. The cross shows the local summer surface wind shear lines. To the equatorward side of the SIO shear line, the monsoon reverses direction during the austral summer (dotted double arrows), so that the anticyclone–ocean interaction becomes a negative feedback to demolish the cold SST off the coast of Sumatra.

b. Theoretical understandings

In the early El Niño development, the A–AM anomalies are primarily induced by the remote ENSO forcing. A distinct feature is the equatorial asymmetry of the A–AM anomalies: A low-level anticyclone extends from the Maritime Continent to the southern tip of India (Fig. 1a). Numerical experiments with a linearized AGCM demonstrate that this asymmetric response is primarily due to the effects of monsoon mean flows on the equatorial wave response (Fig. 6). In particular, the large easterly vertical shear located in the Northern Hemisphere (Fig. 5a) enhance the descending Rossby wave response (Wang and Xie 1996, 1997), leading to a stronger anticyclone ridge to the north of the equator.

The most important point we would like to make is in regard to the critical role of the atmosphere–warm ocean interaction in developing and maintaining the A–AM anomalies. This conclusion was motivated by the following facts. The drastic amplification of the SIO anticyclone in the developing El Niño phases and the ensuing decay toward the mature phase of El Niño cannot be explained solely by the remote El Niño forcing. Neither can it be explained by the persistence of the WNP anticyclone during the decaying El Niño from boreal winter to the next summer.

We propose that the local atmosphere–ocean interaction is principally responsible for the rapid intensification of the SIO anomalous anticyclone in the developing phase and for the maintenance of the WNP anomalous anticyclone in the decay phase of El Niño. The air–sea interaction involved in the SIO and WNP shares a common positive feedback between the moist atmospheric Rossby waves and the mixed layer ocean as described in the schematic diagram (see Fig. 9). The negative SST anomalies to the east of the anticyclone can generate descending atmospheric Rossby waves that enhance the low-level anticyclone in their decaying journey to the west (Gill 1980; Wang et al. 2000). On the other hand, the anomalous anticyclonic winds can generate an SST dipole with cold (warm) anomalies to the east (west) of the anticyclone center through enhanced (reduced) evaporation and entrainment cooling in the presence of favorable background flows (southeast trades in the SIO and northeast trades in the WNP; Figs. 7 and 8). Oceanic processes (e.g., coastal and equatorial upwelling, thermocline fluctuation due to wave adjustment) may further strengthen the anticyclone-induced SST dipole anomalies, especially in the Indian Ocean as discussed in section 5b. It is this positive ocean–atmosphere feedback that can rapidly amplify monsoon and SST dipole anomalies over the Indian Ocean from boreal summer to fall, and develop and maintain monsoon anomalies over the WNP from winter to the ensuing summer, leading to ''prolonged'' impacts of ENSO on the east Asian and WNP monsoons (Wang et al. 2000; Lau et al. 2001). Similar arguments can be applied to a positive feedback between a cyclonic anomaly and an SST dipole with the opposite polarities in the presence of the same background flows.

However, there are differences between the SIO and WNP coupled modes. First, the SIO coupled mode involves more active ocean dynamic effects on SST var-

iation, such as the Java–Sumatra coastal and equatorial upwelling (Saji et al. 1999; Webster et al. 1999), Indonesian throughflow (Susanto et al. 2001), change of the barrier layer due to freshwater fluxes (Saji et al. 1999; AMPXW), and fluctuations of the thermocline due to oceanic wave adjustment (Murtugudde et al. 2000; Xie et al. 2002). Second, the anomalous anticyclone–SST dipole interaction in the SIO is regulated by the background monsoon flow that has pronounced seasonal variation, whereas the mean winds in the WNP are in a relatively stable trade wind regime. The second difference accounts for the dissimilar life spans and seasonality between the SIO and WNP anomalous anticyclones. The fact that the SIO anticyclone has a short duration and matures in northern fall while the WNP anticyclone has a longer duration and lasts for three consecutive seasons is rooted in the different seasonal cycles of the background circulation in the tropical Indian Ocean and the WNP.

c. Discussion

The cooling off the coast of Sumatra along with the broad warming of the western Indian Ocean has been called the Indian Ocean dipole mode (Saji et al. 1999) or zonal mode (Webster et al. 1999). Previous studies of this phenomenon have emphasized the coupling among the SST dipole, the equatorial zonal wind anomalies, and convection dipoles (Saji et al. 1999; Webster et al. 1999; Behera et al. 1999). Our analysis shows that the SIO anticyclone and the dipole SST are the atmospheric and oceanic components of the coupled Indian monsoon–ocean mode. The air–sea coupling is basinwide rather than just near the equatorial Indian Ocean. This coupling involves broadscale, off-equatorial thermodynamic coupling through surface heat flux exchange, which differs in many aspects from the coupling proposed by Bjerknes (1969) for ENSO in the Pacific. The dynamic coupling among the equatorial zonal winds, the SST gradient associated with the SST dipole, and the equatorial upwelling is only a part of the basinwide coupled mode in both the SIO and WNP.

It is conceivable that the positive feedback processes in the tropical Indian Ocean require a sizable kickoff in order for the SST dipole to develop. This is because the cloud–radiation–SST feedback produces a strong damping (Li et al. 2002, manuscript submitted to *J. Atmos. Sci.*, hereafter LWCZ) and because a relatively deep mean thermocline and weak mean equatorial upwelling results in a lack of Bjerknes-type (1969) positive air–sea feedback. Remote El Niño forcing is ideal for triggering the positive feedback between atmospheric Rossby waves and the ocean mixed layer. However, the actual interaction between the monsoon and the underlying ocean described here is, in essence, independent of El Niño forcing. This means that local and other remote forcings may serve as a trigger, such as enhanced convection over Indochina and the South China Sea (LWCZ) or over the Bay of Bengal (Kawamura et al. 2001). Identifying additional triggers during the spring and summer of a developing El Niño is important for predicting the monsoon anomalies associated with the Indian Ocean dipole mode.

The present analysis used 500-hPa vertical *p*-velocity as a surrogate for a tropical convective heat source. The monthly mean precipitation derived from the Climate Prediction Center (CPC) Merged Analysis of Precipitation (CMAP; Xie and Arkin 1997) data were used to check the consistency of the reanalyzed vertical motion with CMAP rainfall. For the same period, 1979–2000, two ESVD modes are obtained: one between the mature phase SST anomaly and 500-hPa vertical *p*-velocity, and the other between the same SST anomaly and CMAP rainfall anomaly. The derived vertical velocity and CMAP rainfall patterns are very similar (figure not shown). The pattern correlation coefficients for the five consecutive seasons are, respectively, -0.62, -0.75, -0.73, -0.71, and -0.58. These results suggest that using the reanalysis 500-hPa vertical motion yields a reasonable estimate of convection anomalies.

The crucial roles of the SIO and WNP anticyclones in generating SST dipole anomalies, as revealed in Figs. 7 and 8, were identified from analyses of the NCEP–NCAR reanalysis data (Kalnay et al. 1996). The uncertainties in the surface heat flux data, however, may lead one to question the quantitative validity of the conclusions. We are currently conducting numerical experiments with a fully coupled atmosphere–ocean model to test the above hypotheses and to investigate the physics of the coupled monsoon–ocean mode and its effects on the climate variation of the A–AM system.

Acknowledgments. The authors thank Dr. G. Speidel for her editorial comments on the manuscript. NOAA CLIVAR/Pacific Program and the Climate Dynamics Program of the National Science Foundation under NSF Award ATM00-73023 have supported this work. IPRC is sponsored in part by the Frontier Research System for Global Change.

REFERENCES

Annamalai, H., R. Murtudde, J. Potema, S.-P. Xie, and B. Wang, 2002: Coupled dynamics in the Indian Ocean: Externally or internally forced? *Deep-Sea Res.*, in press.

Behera, S. K., R. Krishnan, and T. Yamagata, 1999: Unusual ocean–atmosphere conditions in the tropical Indian Ocean during 1994. *Geophys. Res. Lett.,* **26,** 3001–3004.

——, P. S. Salvekar, and T. Yamagata, 2000: Simulation of interannual SST variability in the tropical Indian Ocean. *J. Climate,* **13,** 3487–3499.

Bhalme, H. N., and S. K. Jadhav, 1984: The Southern Oscillation and its relation to the monsoon rainfall. *J. Climatol.,* **4,** 509–520.

Bjerknes, J., 1969: Atmospheric teleconnections from the equatorial Pacific. *Mon. Wea. Rev.,* **97,** 163–172.

Bretherton, C. S., C. Smith, and J. M. Wallace, 1992: An intercomparison of methods for finding coupled patterns in climate data. *J. Climate,* **5,** 541–560.

Chandrasekar, A., and A. Kitoh, 1998: Impact of localized sea surface temperature anomalies over the equatorial Indian Ocean on the Indian summer monsoon. *J. Meteor. Soc. Japan,* **76,** 841–853.
Chang, C.-P., Y. Zhang, and T. Li, 2000: Interannual and interdecadal variations of the east Asian summer monsoon and tropical Pacific SSTs. Part I: Role of the subtropic ridge. *J. Climate,* **13,** 4310–4325.
Chen, L.-X., M. Dong, and Y.-N. Shao, 1992: The characteristics of interannual variations on the East Asian monsoon. *J. Meteor. Soc. Japan,* **70,** 397–421.
Chen, T.-C., S.-P. Weng, N. Yamazaki, and S. Kiehne, 1998: Interannual variation in the tropical cyclone formation over the western North Pacific. *Mon. Wea. Rev.,* **126,** 1080–1090.
Gill, A. E., 1980: Some simple solutions for heat-induced tropical circulation. *Quart. J. Roy. Meteor. Soc.,* **106,** 447–462.
Ju, J., and J. Slingo, 1995: The Asian summer monsoon and ENSO. *Quart. J. Roy. Meteor. Soc.,* **121,** 1133–1168.
Kalnay, E., and Coauthors, 1996: The NCEP/NCAR 40-year Reanalysis Project. *Bull. Amer. Meteor. Soc.,* **77,** 437–471.
Kawamura, R., 1998: A possible mechanism of the Asian summer monsoon–ENSO coupling. *J. Meteor. Soc. Japan,* **76,** 1009–1027.
——, T. Matsuura, and S. Iizuka, 2001: Role of equatorial asymmetric sea surface temperature anomalies in the Indian Ocean on the Asian summer monsoon and El Niño–Southern Oscillation coupling. *J. Geophys. Res.,* **106,** 4681–4693.
Kumar, K. K., B. Rajagopalan, and M. A. Cane, 1999: On the weakening relationship between the Indian monsoon and ENSO. *Science,* **284,** 2156–2159.
Lau, K.-M., and W. R. Bua, 1998: Mechanisms of monsoon–Southern Oscillation coupling: Insights from GCM experiments. *Climate Dyn.,* **14,** 759–799.
——, and H. Weng, 2001: Coherent modes of global SST and summer rainfall over China: An assessment of the regional impacts of the 1997–98 El Niño. *J. Climate,* **14,** 1294–1308.
——, and H. T. Wu, 2001: Principal modes of rainfall–SST variability of the Asian summer monsoon: A reassessment of monsoon–ENSO relationships. *J. Climate,* **14,** 2880–2895.
——, K.-M. Kim, and S. Yang, 2000: Dynamical and boundary forcing characteristics of regional components of the Asian summer monsoon. *J. Climate,* **13,** 2461–2482.
Lau, N.-C., and M. J. Nath, 2000: Impacts of ENSO on the variability of the Asian–Australian monsoons as simulated in GCM experiments. *J. Climate,* **13,** 4287–4309.
——, ——, and H. Wang, 2001: Simulation by a GFDL GCM of ENSO-related variability of the coupled atmosphere–ocean system in the East Asian monsoon region. *World Scientific Publishing Company Book Series on the East Asian Monsoon,* C.-P. Chang, Ed., World Scientific Publishing Series, Vol. 2, World Scientific Publishing Co., in press.
Lindzen, R. S., and N. Nigam, 1987: On the role of sea surface temperature gradients in forcing low-level winds and convergence in the tropics. *J. Atmos. Sci.,* **44,** 2418–2436.
Matsuno, T., 1966: Quasi-geostrophic motions in the equatorial area. *J. Meteor. Soc. Japan,* **44,** 25–42.
Meehl, G. A., 1987: The annual cycle and interannual variability in the tropical Pacific and Indian Ocean region. *Mon. Wea. Rev.,* **115,** 27–50.
Murtugudde, R., J. P. McCreary, and A. J. Busalacchi, 2000: Oceanic processes associated with anomalous events in the Indian Ocean with relevance to 1997–1998. *J. Geophys. Res.,* **105,** 3295–3306.
Nigam, S., 1994: On the dynamical basis for the Asian summer monsoon rainfall–El Niño relationship. *J. Climate,* **7,** 1750–1771.
Nitta, T., 1987: Convective activities in the tropical western Pacific and their impacts on the Northern Hemisphere summer circulation. *J. Meteor. Soc. Japan,* **65,** 373–390.
Palmer, T. N., C. Brankovic, P. Viterbo, and M. J. Miller, 1992: Modeling interannual variations of summer monsoons. *J. Climate,* **5,** 399–417.
Prasad, K. D., and V. Singh, 1996: Seasonal variations of the relationship between some ENSO parameters and Indian rainfall. *Int. J. Climatol.,* **16,** 923–933.
Rao, G. N., 1999: Variations of the SO relationship with summer and winter rainfall over India: 1872–1993. *J. Climate,* **12,** 3486–3495.
Rasmusson, E. M., and T. H. Carpenter, 1982: Variations in tropical sea surface temperature and surface wind fields associated with the Southern Oscillation/El Niño. *Mon. Wea. Rev.,* **110,** 354–384.
——, and ——, 1983: The relationship between the eastern Pacific sea surface temperature and rainfall over India and Sri Lanka. *Mon. Wea. Rev.,* **111,** 517–528.
Reynolds, R. W., and T. M. Smith, 1994: Improved global sea surface temperature analysis using optimum interpolation. *J. Climate,* **7,** 929–948.
Saji, N. H., B. N. Goswami, P. N. Vinayachandran, and T. Yamagata, 1999: A dipole mode in the tropical Indian Ocean. *Nature,* **401,** 360–363.
Shen, S., and K.-M. Lau, 1995: Biennial oscillation associated with the East Asian summer monsoon and tropical Pacific sea surface temperatures. *J. Meteor. Soc. Japan,* **73,** 105–124.
Shukla, J., and D. A. Paolino, 1983: The Southern Oscillation and long-range forecasting of the summer monsoon anomalies over India. *Mon. Wea. Rev.,* **111,** 1830–1837.
——, and J. M. Wallace, 1983: Numerical simulation of the atmospheric response to equatorial sea surface temperature anomalies. *J. Atmos. Sci.,* **40,** 1613–1630.
Slingo, J. M., and H. Annamalai, 2000: 1997: The El Niño of the century and the response of the Indian summer monsoon. *Mon. Wea. Rev.,* **128,** 1778–1797.
Soman, M. K., and J. Slingo, 1997: Sensitivity of the Asian summer monsoon to aspects of sea-surface temperature anomalies in the tropical Pacific Ocean. *Quart. J. Roy. Meteor. Soc.,* **123,** 309–336.
Susanto, R. D., A. L. Gordon, and Q. Zheng, 2001: Upwelling along the coasts of Java and Sumatra and its relation to ENSO. *Geophys. Res. Lett.,* **28,** 1599–1602.
Tanaka, M., 1997: Interannual and interdecadal variations of the western North Pacific monsoon and the East Asian Baiu rainfall and their relationship to ENSO cycles. *J. Meteor. Soc. Japan,* **75,** 1109–1123.
Ting, M., and L. Yu, 1998: Steady response to tropical heating in wavy linear and nonlinear baroclinic models. *J. Atmos. Sci.,* **55,** 3565–3582.
Wang, B., 1995: Transition from a cold to a warm state of the El Niño–Southern Oscillation cycles. *Meteor. Atmos. Phys.,* **56,** 17–32.
——, and T. Li, 1993: A simple tropical atmospheric model of relevance to short-term climate variation. *J. Atmos. Sci.,* **50,** 260–284.
——, and X. Xie, 1996: Low-frequency equatorial waves in sheared zonal flow. Part I: Stable waves. *J. Atmos. Sci.,* **53,** 449–467.
——, and ——, 1997: A model for boreal summer intraseasonal oscillation. *J. Atmos. Sci.,* **54,** 72–86.
——, and Z. Fan, 1999: Choice of South Asian monsoon indices. *Bull. Amer. Meteor. Soc.,* **80,** 629–638.
——, and J. C. L. Chan, 2002: How strong ENSO events affect tropical storm activity over the western North Pacific. *J. Climate,* **15,** 1643–1658.
——, and Q. Zhang, 2002: Pacific–east Asian teleconnection. Part II: How the Philippine Sea anomalous anticyclone is established during El Niño development. *J. Climate,* **15,** 3252–3265.
——, R. Wu, and X. Fu, 2000: Pacific–east Asian teleconnection: How does ENSO affect east Asian climate? *J. Climate,* **13,** 1517–1536.
——, ——, and K.-M. Lau, 2001: Interannual variability of the Asian summer monsoon: Contrasts between the Indian and the western North Pacific–east Asian monsoons. *J. Climate,* **14,** 4073–4090.
Weare, B. C., and J. S. Nasstrom, 1982: Examples of extended em-

pirical orthogonal function analyses. *Mon. Wea. Rev.,* **110,** 481–485.
Webster, P. J., and S. Yang, 1992: Monsoon and ENSO: Selectively interactive systems. *Quart. J. Roy. Meteor. Soc.*, **118,** 877–926.
——, V. O. Magaña, T. N. Palmer, R. A. Thomas, M. Yanai, and T. Yasunari, 1998: Monsoons: Processes, predictability, and the prospects for prediction. *J. Geophys. Res.*, **103,** 14 451–14 510.
——, A. M. Moore, J. P. Loschnigg, and R. R. Leben, 1999: The great Indian Ocean warming of 1997–98: Evidence of coupled oceanic–atmospheric instabilities. *Nature,* **401,** 356–360.
Xie, P., and P. A. Arkin, 1997: Global precipitation: A 17-year monthly analysis based on gauge observations, satellite estimates, and numerical outputs. *Bull. Amer. Meteor. Soc.*, **78,** 2539–2558.
Xie, S.-P., H. Annamalai, F. A. Schott, and J. P. McCreary, 2002: Structure and mechanisms of South Indian Ocean climate variability. *J. Climate,* **15,** 864–878.
Xie, X., and B. Wang, 1996: Low-frequency equatorial waves in vertically sheared zonal flows. Part II: Unstable waves. *J. Atmos. Sci.*, **53,** 3589–3605.
Yang, S., and K.-M. Lau, 1998: Influence of sea surface temperature and ground wetness on Asian summer monsoon. *J. Climate,* **11,** 3230–3246.
Ye, D.-Z., and R.-H. Huang, 1996: *Study in the Regularity and Formation Reason of Drought and Flood in the Yangtze and Huaihe River Regions* (in Chinese). Shandon Science and Technology Press, 387 pp.
Zebiak, S. E., 1986: Atmospheric convergence feedback in a simple model for El Niño. *Mon. Wea. Rev.,* **114,** 1263–1271.
Zhang, R., A. Sumi, and M. Kimoto, 1999: A diagnostic study of the impact of El Niño on the precipitation in China. *Adv. Atmos. Sci.,* **16,** 229–241.